

On the Mass Assembly History of the Local Group

Edoardo Carlesi¹, * Yehuda Hoffman², Stefan Gottlöber¹, Noam I. Libeskind^{1,3},
Alexander Knebe^{4,5,6}, Gustavo Yepes^{4,5}, Sergey V. Pilipenko⁷

¹Leibniz-Institut für Astrophysik Potsdam (AIP), An der Sternwarte 16, D-14482 Potsdam, Germany

²Racah Institute of Physics, Givat Ram, 91040 Jerusalem, Israel

³University of Lyon, UCB Lyon 1, CNRS/IN2P3, IPN Lyon, 69622 Villeurbanne, France

⁴Departamento de Física Teórica, Módulo 8, Facultad de Ciencias, Universidad Autónoma de Madrid, 28049 Madrid, Spain

⁵Centro de Investigación Avanzada en Física Fundamental (CIAFF), Facultad de Ciencias, Universidad Autónoma de Madrid, 28049 Madrid, Spain

⁶International Centre for Radio Astronomy Research, University of Western Australia, 35 Stirling Highway, Crawley, Western Australia 6009, Australia

⁷Astro Space centre of Lebedev Physical Institute of Russian Academy of Sciences, Profsojuznaja st. 84/32, 117997 Moscow, Russia

Submitted XXXX May XXXX

ABSTRACT

In this work an ensemble of simulated Local Group analogues is used to constrain the properties of the mass assembly history of the Milky Way (MW) and Andromeda (M31) galaxies. These objects have been obtained using the constrained simulation technique, which ensures that simulated LGs live within a large scale environment akin to the observed one. Our results are compared against a standard Λ Cold Dark Matter (Λ CDM) series of simulations which use the same cosmological parameters. This allows us to single out the effects of the constraints on the results. We find that (a) the median constrained merging histories for M31 and MW live above the standard ones at the $1-\sigma$ level, (b) the median formation time takes place ≈ 0.5 Gyr earlier than unconstrained values, while the latest major merger happens on average 1.5 Gyr earlier and (c) the probability for both LG haloes to have experienced their last major merger in the first half of the history of the Universe is $\approx 50\%$ higher for the constrained pairs. These results have been estimated to be significant at the 99% confidence level by means of a Kolmogorov-Smirnov test. These results suggest that the particular environment in which the Milky Way and Andromeda form plays a role in shaping their properties, and favours earlier formation and last major merger time values in agreement with other observational and theoretical considerations.

Key words: Cosmology, Numerical simulations, Dark matter, Local Group

1 INTRODUCTION

The two main galaxies of the Local Group (LG), known as the Milky Way (MW) and Andromeda (M31), play a crucial role in shaping our understanding of galaxies in general. Due to their proximity, the large amount of high-quality data available for these two disk galaxies, has given rise to so-called near field cosmology (Bland-Hawthorn & Peebles 2006; Bland-Hawthorn & Freeman 2014), an approach that aims at extracting cosmological information by observing the cosmic near-field. A number of studies have shown that by analysing the LG through a cosmological lens it is possible to understand, test and constrain the paradigm of galaxy and structure formation, the Λ Cold Dark Matter (Λ CDM) model (de Rossi et al. 2009; Boylan-Kolchin et al. 2010, 2012; Zavala et al. 2012; Forero-Romero et al. 2013; Garrison-Kimmel

et al. 2014; Tollerud et al. 2014) as well as non-standard, alternative theories (Elahi et al. 2015; Penzo et al. 2016; Garaldi et al. 2016; Carlesi et al. 2017b).

The location of a dark matter (DM) halo within a specific environment in the cosmic web has been suggested to play an important role in shaping galaxies properties, such as its morphological type (Dressler 1980; Nuza et al. 2014; Metuki et al. 2015) and star formation rates, which for MW-like galaxies are affected by higher-density environments (Creasey et al. 2015). Moreover, the filamentary nature of the LG surroundings affects its evolution through ram pressure stripping (Benitez-Llambay et al. 2013) on the one hand and feeding it with cold streams of gas (Aragon-Calvo et al. 2016) on the other, while is also linked to the anisotropic distribution of the MW and M31 satellites (Libeskind et al. 2015a).

In the hierarchical picture of structure formation, where smaller DM haloes gradually merge into larger ones (White & Rees 1978),

* E-mail: ecarlesi@aip.de

the properties of galaxies may strongly depend on their host and the way it has accreted its mass (Parry et al. 2009; Stinson et al. 2010; van Dokkum et al. 2013; Rodríguez-Gomez et al. 2017). In particular, the formation of disks such as those observed in MW and M31, in a Λ CDM cosmology, is crucially linked to the mass assembly history (MAH) of their DM haloes (Toth & Ostriker 1992; Brook et al. 2005; Naab & Ostriker 2006; Forero-Romero et al. 2011; Sales et al. 2012), since recent collisions with massive galaxies can inhibit their formation (Brook et al. 2004; Stewart et al. 2008; Scannapieco et al. 2009; Hammer et al. 2012; Scannapieco et al. 2015); an observation which is also confirmed by the properties of the white dwarf luminosity functions (Kilic et al. 2017). Moreover, the angular momentum and stellar mass of the MW suggest that no significant merger¹ took place in the last 8 to 10 Gyr (Hammer et al. 2007; Ruchti et al. 2015). More recently, Helmi et al. (2018) and Iorio & Belokurov (2019), using Gaia data, could identify a large galaxy that merged with the MW’s main progenitor around 10 Gyrs ago; this now fully coalesced galaxy, called Gaia-Enceladus, would be the latest massive object to have merged with the Galaxy. The most recent merging event experienced by the MW is most likely represented by the dwarf spheroidal galaxy Sagittarius (Sgr), which might be responsible the vertical oscillations of the disk (Laporte & et al. 2018); the actual value of its progenitor’s mass is actually unknown though it could be as massive as $10^{11} M_{\odot}$, in which case it would classify as a major merger according to our definition. Moreover, from the point of view of the MW dark matter halo, there is an ongoing interaction with the Large Magellanic Cloud (LMC), whose mass is estimated to be as large as 20% of the MW (Peñarrubia et al. 2016). However, being on its first crossing of the viral radius (Besla et al. 2007; Kallivayalil et al. 2013) the LMC did not have enough time to perturb the disk of the MW (Mastropietro et al. 2005), though a future LMC-MW merger is quite likely inevitable and will affect the properties of the bulge and the stellar halo significantly (Cautun et al. 2018).

In the case of M31, where both the properties of its bulge (Hammer et al. 2010) and possibly also the anisotropic distribution of the satellites (Fouquet et al. 2012; Hammer et al. 2013), suggest that a major merger took place around $\approx 7 - 8$ Gyr ago at the latest, while a number of studies based primarily on the age of stars in M31’s bulge, claim that such an event took place as early as 10 – 11 Gyr ago (Brown et al. 2008; Saglia et al. 2010; Dalcanton et al. 2012). It needs to be noted, however, that in contrast with the previous works Hammer et al. (2018) found that M31’s thick disk might have originated from a merger of a large satellite which fully coalesced only around 1.8 – 3 GYrs ago. In general, however, there is a broad, theoretically and observationally motivated, consensus that the LG is characterized by a substantially quiet merging history during the last few gigayears.

Hence, it is fundamental to keep in mind this considerations on the environment and MAH of the LG when practicing near field cosmology using N -body simulations.

A popular way of addressing this kind of studies is represented by the constrained simulation (CS) technique, that aims at reproducing the $z = 0$ Universe, in order to allow for a direct comparison of the simulation’s output and observations (Gottlöber

Table 1. Median and variance for the three shear tensor eigenvalues in CS and RAN.

	RAN	CS
λ_1	0.47 ± 0.23	0.16 ± 0.03
λ_2	0.14 ± 0.23	0.06 ± 0.01
λ_3	-0.29 ± 0.07	-0.14 ± 0.01

et al. 2010; Sorce et al. 2014; Wang et al. 2016; Sorce et al. 2016). Based on these approach, Carlesi et al. (2016a) have developed the so called *Local Group factory*, a numerical pipeline that allows to produce pairs of LG-like haloes in a large scale environment which closely mimics the observed one, within the framework of the Constrained Local UniversE Simulation (CLUES) project². This tool has been used to simulate a series of LGs, which are used in this work to reconstruct the merger history of MW and M31, comparing them to those obtained for a control-group of similar objects identified in a standard random-phase Λ CDM simulation (RAN). The focus is placed on MW and M31, the most prominent members of the LG, and on their MAH, using two metrics to do so: the last major merger time (τ_M) and the moment when each halo acquired half its $z = 0$ mass, defined as its formation time (τ_F). Our approach in this work is close to the one of Forero-Romero et al. (2011), however, the significantly larger sample of constrained LGs allows us to put our conclusions on a firmer statistical footing.

This work is structured as follows. Section 2 contains a description of the simulations and the methods used, discussing also the definition of LG in cosmological simulations. In Section 3 we compute the median MAHs for MW and M31 and derive distribution functions for τ_F and τ_M , highlighting the differences between the CS and RAN and discussing their consequences. In Section 4 we summarize our main results, discussing their implications and their relation to the current observational and theoretical status.

2 METHODS

This work is based on two different sets of N -body simulations, for standard Λ CDM (labeled RAN) and CSs, both run using Planck-I cosmological parameters: $\Omega_m = 0.31$, $\Omega_{\Lambda} = 0.69$, $h = 0.67$ and $\sigma_8 = 0.83$ (Planck Collaboration 2014), a box of $100h^{-1}\text{Mpc}$, a mass resolution of $8 \times 10^7 h^{-1}M_{\odot}$ and a smoothing length of $2h^{-1}\text{kpc}$. For the RAN simulation five 1024^3 particle simulations were ran, while due to the large number of CSs needed to produce a significant sample size, a zoom-in technique was used for a $\approx 7h^{-1}\text{Mpc}$ sphere around the center of a $100h^{-1}\text{Mpc}$ box (with a resolution equivalent to 1024^3 in the full box) using the G \ddot{u} nnungagap³ code. Each simulation has stored a total of 54 snapshots, at constant separation of 250 Myr from $z_{init} = 80$ to $z = 0$. The following paragraphs will describe the main properties of the simulations and their relevance for the issue investigated here.

¹ A major merger is defined in this paper as a merger where the mass ratio between the two halos is at least 1 : 10.

² <http://www.clues-project.org>

³ <https://github.com/ginnungagapgroup/ginnungagap>

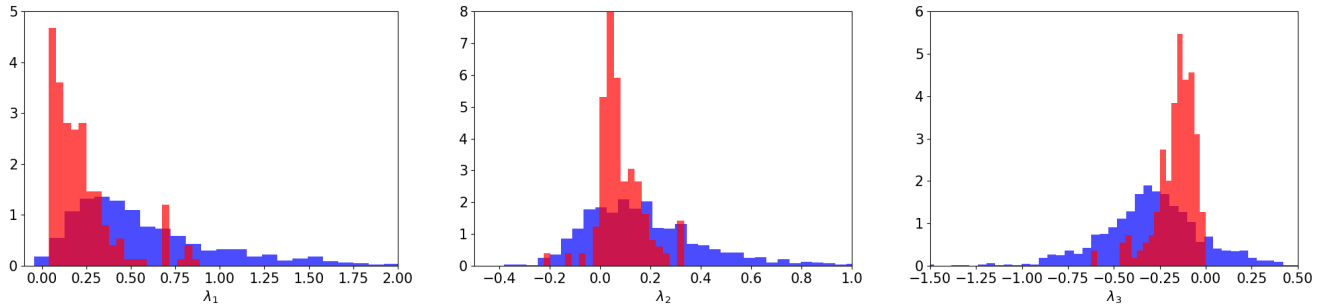


Figure 1. Distribution of the velocity shear tensor eigenvalues λ_1 , λ_2 and λ_3 computed at the position of the LG center of mass, for CS (red color) and RAN (in blue) samples. The area under the curve is normalized to 1. We note that the λ s are much more tightly distributed around the mean in CS simulation than in RAN.

2.1 The Simulations

Constrained simulations These are cosmological simulations whose initial conditions (ICs) have been manipulated such that specific $z = 0$ cosmographic constraints, set by observations of the local universe, are met. By “cosmographic constraints” we mean local gravitational sources such as the Virgo cluster. These constraints are given by the (grouped) Cosmic Flows 2 peculiar velocity data catalog (Tully et al. 2014), using the procedure of Sorce (2015) to minimize observational biases. Coupled with the Wiener filter technique and constrained realization of a Gaussian field algorithm (Hoffman & Ribak 1991), these data allow to reconstruct the velocity and density field at $z = 0$. Constrained ICs are then generated by scaling the field back to the starting redshift ($z = 80$ in our case) using the Reverse Zeldovich Approximation described by Doumler et al. (2013a,b,c). Peculiar velocity constraints are mostly effective on scales above $\approx 4h^{-1}\text{Mpc}$, meaning that below this threshold the random modes are expected to dominate. Carlesi et al. (2016a) have shown that it is possible to optimize the above techniques to produce a numerical pipeline (the *Local Group Factory*, LGF) that produces LG-like DM halo pairs at substantially higher rate than expected by applying similar identification criteria to large cosmological volumes – this despite the major role played by the random component on these scales. This large sample of halo pairs, which lie in an environment akin to the observed one, can be used to constrain the dynamics of the LG, linking its mass and velocity to the cosmological and large scale context (Carlesi et al. 2016b, 2017a). In this work, we will use a subset of 314 pairs selected from the first series of the LGF simulations according to criteria laid out in the following section.

The results drawn from these halo sample were compared to a second LG-like sample of objects, found in a standard random realization of the ΛCDM model (RAN).

Random simulations In order to provide for a consistent control sample of dark matter haloes, a series of five full box simulations implementing exactly the same simulation setup as the CSs (apart from the application of zoom-in region). In each of the simulations it was possible to identify ~ 400 LG-like halo pairs (using the criteria outlined in Section 2.3) and resulting in a total of 2028 objects for the RAN control sample.

2.2 Halo Catalogs and Merger Trees

All the simulations have been analyzed using the same merger tree algorithm and halo finding software. Halo catalogs are produced

for each snapshot using the AHF spherical overdensity halo finder (Knollmann & Knebe 2009). The merger trees are derived using the METROC++ code, which can be freely downloaded from <https://github.com/EdoardoCarlesi/MetroCPP>. METROC++ stands for *MErger TRees On C++*, and its main properties are described in Appendix A. The merger trees obtained have been smoothed in the post-processing phase removing spurious mass accretion due to halo fly-bys.

2.3 The Local Group Model

The parameters and intervals used to define a simulated LG vary substantially among different authors (e.g. Forero-Romero et al. 2013; González et al. 2014; Sawala et al. 2014; Libeskind et al. 2015a; Fattahi et al. 2016), affecting at least to some extent the conclusions reached. It is therefore necessary to single out and motivate the specific choice made, which constitute a *prior* or - using the terminology introduced in Carlesi et al. (2016b), a Local Group model. While any choice of the priors is generally related to the observational properties of the system, this needs to be flexible enough to allow for a statistically significant sample of haloes to be built. In this work, LG candidates are identified using the following criteria

- Halo mass $> 0.5 \times 10^{12} h^{-1} M_{\odot}$
- Total mass below $5.0 \times 10^{12} h^{-1} M_{\odot}$
- Halo separation in the range $(0.35 - 1.25) h^{-1} \text{Mpc}$
- Mass ratio $M_{M31} / M_{MW} < 3.0$
- Negative radial velocity
- Isolation, i.e., no third halo of mass $\geq M_{MW}$ is located within $2.5 h^{-1} \text{Mpc}$ from the center of mass of the LG

We focus only on the two largest LG members, labeling the least (most) massive member as MW (M31) (see Baiesi Pillastrini 2009; Karachentsev et al. 2009; Diaz et al. 2014). Given widely different values for the tangential motion of the M31 in the literature (Sohn et al. 2012; Salomon et al. 2016; Carlesi et al. 2016b; van der Marel et al. 2019), we allow for a large range of v_{tan} values, that are consistent with the state-of-the-art. Moreover to avoid biasing our results by comparing different mass ranges, we ensure that the distributions of M_{MW} , M_{M31} and M_{LG} converge to the same median values in both samples as shown by (Carlesi et al. 2017a).

2.4 The environment

The main difference between LG-like objects in the constrained simulation set is given by the *environment*, which can be classified

using several different schemes such as those based on the tidal tensor (Aragón-Calvo et al. 2007; Hahn et al. 2007; Forero-Romero et al. 2009), watershed segmentation (Aragón-Calvo et al. 2010), the velocity shear tensor (Hoffman et al. 2012), Bayesian reconstruction using tracers of the density field (Leclercq et al. 2015) among the others. Here we implemented the classification algorithm of Hoffman et al. (2012) which classifies the environment in terms of the eigenvalues λ_i of the velocity shear tensor:

$$\Sigma_{\alpha\beta} = -\frac{1}{2H_0} \left(\frac{\partial v_\alpha}{\partial r_\beta} - \frac{\partial v_\beta}{\partial r_\alpha} \right) \quad (1)$$

In this formalism, a given point in space is classified as a *void* if the three eigenvalues are below a given threshold λ_{th} ; it is labeled as a *sheet* when two of eigenvalues are $< \lambda_{th}$, it is called a *filament* when one eigenvalue is $< \lambda_{th}$ and a *knot* when all of the eigenvalues are $> \lambda_{th}$. As shown in Carlesi et al. (2016a) using a $2.5h^{-1}\text{Mpc}$ smoothing, these eigenvalues are very well constrained at the position of the LG center of mass, where the environment is classified as a filament according to our definition. In this work, we used a 64^3 regular grid and a $1.5 h^{-1}\text{Mpc}$ smoothing length in all the RAN and CS simulation boxes to compute the λ s; in Fig. 1 we plot their values at the nearest grid point to each of the simulated LG. This quantitatively shows the differences among the two samples, where the constrained nature of the CS is reflected in the substantially smaller scatter. The mean values together with their variance are shown in Table 1; these values are in very good agreement with those obtained reconstructed by Libeskind et al. (2015b). Imposing the condition that the three eigenvalues around the LGs of the RAN simulations simultaneously lie within $\pm 2\sigma$ around the median CS λ_1 , λ_2 and λ_3 from Table 1, it turns out that (despite the large overlap between the two distributions) only 8 out of 2028 pairs can be selected. Hence, while qualitatively RAN and CS samples live in similar kinds of environment, applying stricter quantitative criteria on the properties of the shear tensor around candidate local groups leads to a remarkable shrinking of the halo mple.

3 RESULTS

The sample of 2028 LG-like pairs identified in the RAN simulations functions as a benchmark to highlight the effect of the constrained environment on

- the mass assembly history
- formation time
- last major merger time

that are going to be defined and discussed in the following subsections.

3.1 Mass Assembly History

Our reconstruction of the halo history includes both smooth accretion of individual DM particles not bound into any discernible structure other well resolved haloes. Using the CS and RAN halo samples and the LG model to identify MW and M31 like-objects, we compute the *median* MAH together with its 25th and 75th percentile intervals, shown in Fig. 2. We observe that, despite the significant overlap between the two distributions, in both MW

Table 2. Best fit values for the α and β parameters of Eq. (2) for MW and M31, obtained using the CS and RAN LG samples.

	MW(CS)	MW(RAN)	M31(CS)	M31(RAN)
α	$5.54^{+0.24}_{-0.30}$	$6.24^{+0.32}_{-0.45}$	$6.01^{+0.22}_{-0.29}$	$6.33^{+0.33}_{-0.27}$
β	$2.71^{+0.18}_{-0.11}$	$2.71^{+0.07}_{-0.23}$	$2.66^{+0.16}_{-0.09}$	$2.91^{+0.11}_{-0.14}$

and M31, the median values computed with the CS sample differ significantly from the RAN ones at the 1σ level. Specifically, the median mass of LGs forming in constrained simulations, is larger at early times compared to “random” LGs. This is a clear difference between the two samples, providing a first hint of the influence of the environment on the formation history of the LG. As can be seen in the last 6 Gyr, in fact, $\approx 50\%$ of the CS LGs can be characterized by an MAH which lies above the 75th percentile of the unconstrained ΛCDM distribution. This means that haloes whose MAH lies within the residual 25th percentile of the distributions are expected to be seen twice as many times when introducing environmental constraints. Such a finding is in qualitative agreement with the results of Forero-Romero et al. (2011), who also found that CS MAHs consistently lied above the RAN expectations.

It is important to note that LGs identified in the CSs, are not – as a rule – more massive than their RAN counterparts. That they fulfill the same $z = 0$ mass criteria is by construction. But it is important to note that at early times, at look back times of say ~ 10 or 11 Gyr, the main progenitor of both the MW and M31 in both CS and RAN, have roughly the same mass of 0.15 (in units of the $z = 0$ MW and M31 mass). In other words at the earliest epochs the samples have assembled similar amounts of their $z = 0$ mass; the LGs in the CS grow faster at first and then their growth slows, while LGs in RAN grow slower at first and then faster at late cosmic times, ensuring that by $z = 0$ the samples fulfill the same mass criterium.

Many authors (see e.g. Tasitsiomi et al. 2004; McBride et al. 2009; Boylan-Kolchin et al. 2010) have found that the MAH of a DM halo is well fit by a modified exponential function of the kind

$$\frac{M(z)}{M_0} = (1+z)^\beta \exp(-\alpha(\sqrt{1+z} - 1)) \quad (2)$$

We fit this function for MW and M31 in the two halo samples, finding the parameters shown in Table 2. In both cases, the difference between the numerical MAH and the analytical best-fit prediction is computed to be less than 2%. As expected, the α values obtained for the CS haloes are smaller than those found in RAN reflecting the quieter accretion history that characterizes constrained MWs and M31s. These results can be compared to the findings of Boylan-Kolchin et al. (2010) and Forero-Romero et al. (2011). These authors quoted a different set of best fit values, with $\alpha = 2.23$ and β , which they found to be 4.90 and 4.50, respectively. However, such a discrepancy can be expected since (a) the halo sample used by the aforementioned authors spans over a wider mass range, (b) the cosmological parameters were WMAP1 and WMAP5 instead of Planck-I (c) the FoF halo finding method is a major source of differences in the MAH, with respect to the spherical overdensity (see Avila et al. 2014) and (d) the function is fitted over a different redshift range (0 to 3 instead of 0 to 10). We estimate the discrep-

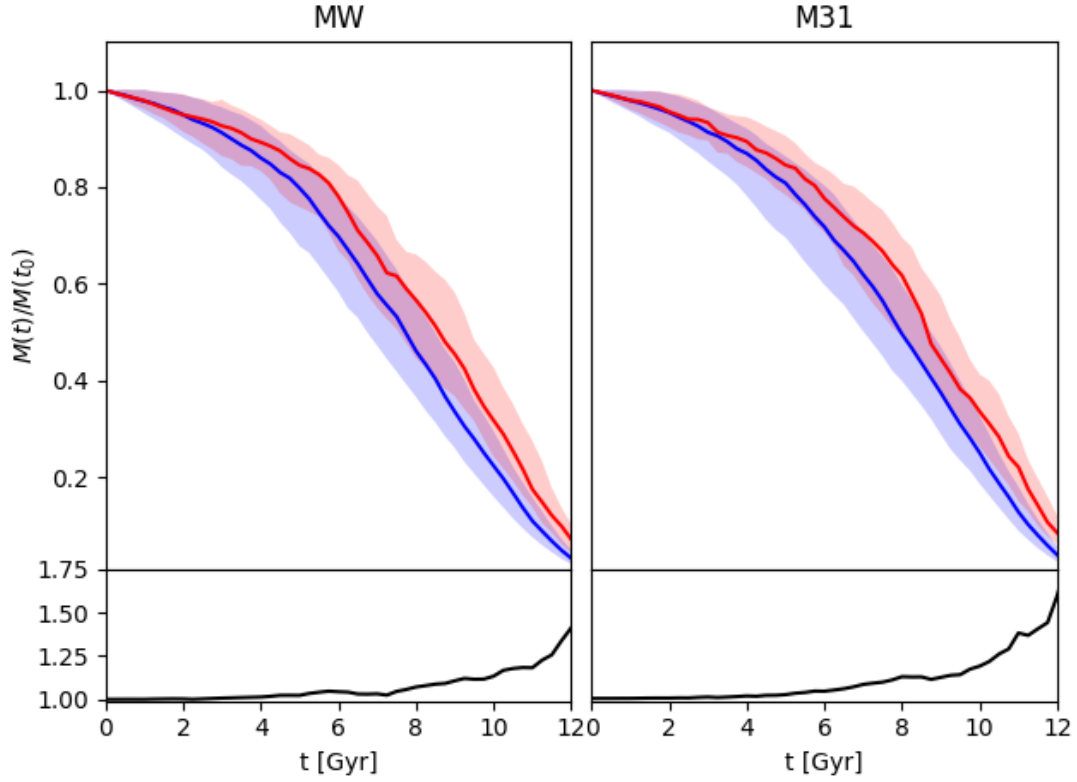


Figure 2. Mass assembly histories for MW and M31 for both the CS (red) and RAN (blue) samples; showing their median values (thick lines) and their 25 – th and 75 – th percentiles (shaded region).

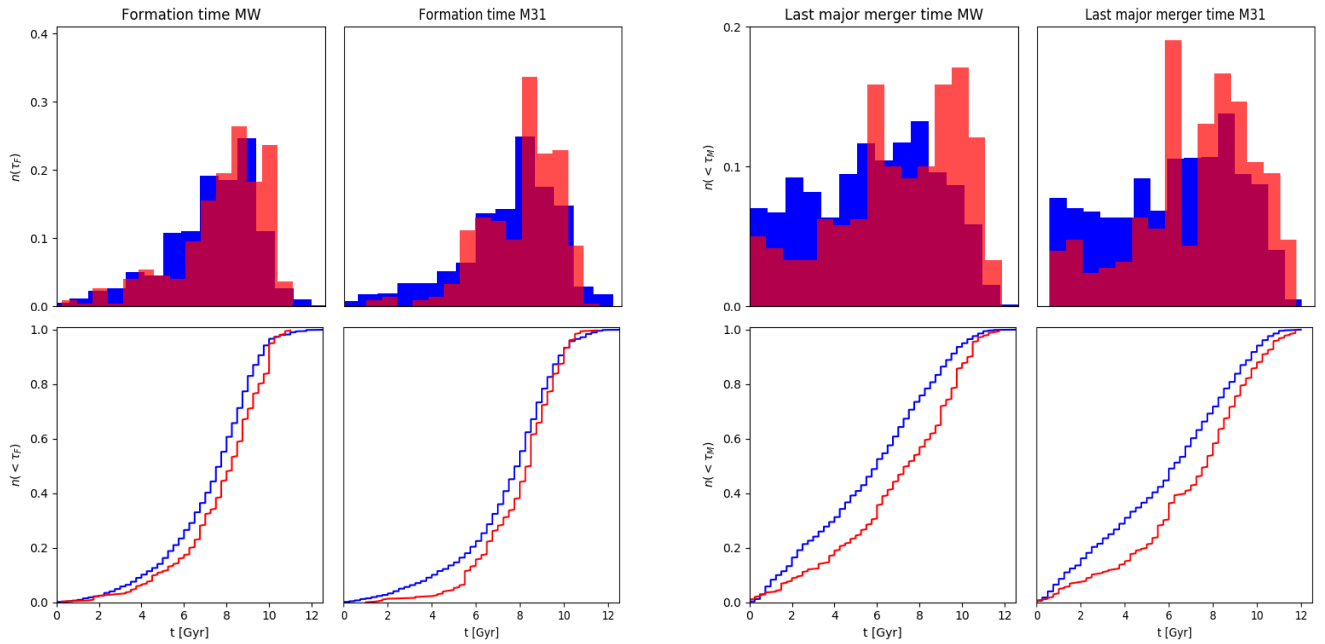


Figure 3. Formation and last major merger times (τ_M) for MW and M31; histograms (upper panels) and cumulative distribution (lower panels). Red (blue) colors are for the CS (RAN) sample, while x -axis is in Gyr lookback time units.

Table 3. Median values of the τ_F (left table) and τ_M (right table) distributions for MW and M31 haloes, in the CS and RAN samples, with the relative 25th and 75th percentile intervals. Units are in Gyr lookback time

	τ_F		τ_M	
	CS	RAN	CS	RAN
MW	$8.50^{+0.75}_{-2.25}$	$8.00^{+1.00}_{-1.75}$	$7.75^{+1.25}_{-2.25}$	$6.25^{+2.00}_{-2.75}$
M31	$8.25^{+1.00}_{-1.50}$	$7.75^{+1.00}_{-1.75}$	$7.50^{+2.00}_{-2.25}$	$6.00^{+2.00}_{-2.75}$

ancy between our values and the aforementioned ones computing root mean square difference (Δ_{RMS}) of Eq. (2) over an interval $z = [0.0 - 6.0]$. Using different combinations of α s and β s of Table 2 versus the best fit formulas of Boylan-Kolchin et al. (2010) and Forero-Romero et al. (2011) we see that Δ_{RMS} varies in the interval 0.08 – 0.28 across the different combinations. These numbers are of the same order of magnitude of those obtained comparing the different MW/M31 (CS/RAN) α , β values of Table 2, which give e.g. $\Delta_{RMS} = 0.18$ in the case of MW(CS) and M31(RAN). The implications of a flatter MAH for the expected values of τ_M and τ_F will be discussed in the following subsections.

3.2 Formation Times

Halo formation time τ_F is defined in this work as the time at which the main branch of the merger tree has reached half of the $z = 0$ mass of the DM halo. We compute this quantity for each of the LG in the CS and RAN samples and plot the τ_F distribution in Fig. 3. The median τ_F values for all the distributions are shown in Table 3. In agreement with the findings of the previous subsection, CS haloes are characterized by median τ_F values which are ≈ 0.5 Gyr above the RAN expectations. This can be seen in Fig. 3, where the distributions are shifted at slightly higher lookback time values, with a more pronounced peak at ≈ 8 Gyr for both haloes. We complete the analysis computing the fraction of haloes that formed within the first half ($\tau_{1/2} = 6.9$ Gyr lookback time) and within the first quarter ($\tau_{3/4} = 10.35$ Gyr lookback time) of the age of the Universe. In the first case, we find an excess probability 8% – 15% of CS MWs, M31s and LGs to have formed in that time range; with a large overlap of the values as shown in Fig. 3. In the second case, however, it can be noticed that the shift of the medians of the CS distributions leaves a sizable amount of objects with a very early τ_F , whose expected number is almost negligible the RAN sample. Nonetheless, the overall picture tells us that the environment-induced bias here is subdominant and the very large overlap between the distributions coming from the different samples indicates that the τ_F is essentially determined by the halo mass. In fact, it can be noticed that MWs have earlier τ_F s than M31 in both samples, consistent with the hierarchical formation picture and our LG model which prescribed $M_{M31} > M_{MW}$.

To conclude the section, we compare these results with the τ_F distributions of Forero-Romero et al. (2011), who computed them using the Bolshoi simulation (Klypin et al. 2011). In that case, it turned out that individual haloes over a mass range comparable to the one of MW and M31 in the RAN simulation, for τ_F lookback times > 9 Gyr, represent the 23% – 29% of the sample, and around 5% of the total number of LG-like pairs. Applying this

threshold to RAN, we find that MW and M31 have $\tau_F > 9$ Gyr in 26% and 22% of the times respectively, while the share of LGs with both main haloes satisfying this criterion is $\approx 4\%$, showing that our benchmark rates broadly agree with those already existing in the literature.

3.3 Last Major Merger

Following Forero-Romero et al. (2011), we define as *major merger* any merger event where mass of the accreted halo has a ratio of at least 1:10 with respect to the main one. The parameter τ_M is defined as the age of the universe/lookback time when such an event last took place. As for τ_F , we show the distributions of both samples for τ_M in Fig. 3. First, we notice that the median values presented in Table 3 show that CS estimate are 1.5 Gyr above the RAN ones, i.e. 7.75 for MW and 7.50 for M31. This means that the expected merger history is consistently more quiet when simulating LGs in their correct environment. The significance of this difference observed among the two distributions of the τ_M values can be evaluated by means of a Kolmogorov-Smirnov (KS) test using the cumulative distributions shown in the lower panels of Fig. 3. The p -values for MW and M31 are 2.42×10^{-6} and 1.56×10^{-4} respectively, so that the null hypothesis that the two τ_M samples come from the same distribution can be rejected at the $> 99\%$ level. For comparison, the p -values for the KS test in the case of τ_F are both ≈ 0.21 . We then estimate the effect of the sample size (which is substantially smaller for CS) in the following way. Randomly drawing 10000 subsamples of $N = 314$ from the 2028 RAN pairs, we repeating the KS test for each one using the complete RAN distribution, and look at the p -values obtained. It is found that only less than 0.007% of the times the τ_M for the reduced RAN subsample (for both MW and M31) has a p -value smaller than 0.05, allowing us to conclude that a random fluctuation is extremely unlikely to explain estimated the p -value.

To further quantify the incompatibility introduced by the constraints, we focus again on the first half and the first quarter of the age of the Universe and compute the fractions of haloes whose τ_M falls within the two intervals, which are shown in Table 4. Those haloes whose last major merger time falls within the first interval are said to have a *quiet* merging history whereas the second group has an *extremely quiet* one. In the first case, the effect of the CS is evident: the rates of MW and M31 experiencing a last major merger in this time interval is up to 20% larger than RAN rates. Moreover, more than a quarter of the LGs can be characterized by this kind of τ_M s, a value which is twice as large as LGs identified in unconstrained Λ CDM simulations, showing that the effect of the constraints is to force the sample towards a *quiet* merger history.

On the other hand, the size of this effect is diminished in the case of haloes with an extremely quiet merger history. In this case the fractions of the samples are of comparable size between RAN and CS, with slightly higher values for the CS haloes. Taking a perhaps more realistic approach, we can use two different τ_M and compute probabilities for the combined MW + M31 system for a more realistic set of priors. Analysing the angular momentum, stellar mass and properties of the disk of the Hammer et al. (2007) concluded that MW experienced its last major merger ≈ 10 Gyr for MW; while Hammer et al. (2010) suggested that the bulge, disk and thick disk structure of lead to $\tau_M \approx 8.75$ Gyr for M31. Applying these two combined values it is found that such a configuration is realised in $\approx 6\%$ and 4% of the times for the CS and RAN samples; the excess probability in this case is not

Table 4. Fraction of haloes that formed (τ_F) and experienced their latest major merger (τ_M) in the first half ($\tau_{1/2}$) and the first quarter (that is $\tau_{3/4}$ in lookback time) of the age of the Universe. The values are computed for individual MW and M31 as well as for the whole LG, i.e. when both haloes in the pair form or experience a merger at a time smaller than $\tau_{3/4}$ or $\tau_{1/2}$.

	$n(\tau_F > \tau_{1/2})$		$n(\tau_F > \tau_{3/4})$		$n(\tau_M > \tau_{1/2})$		$n(\tau_M > \tau_{3/4})$	
	CS	RAN	CS	RAN	CS	RAN	CS	RAN
MW	0.77	0.67	0.16	0.06	0.60	0.46	0.18	0.09
M31	0.76	0.71	0.12	0.08	0.58	0.41	0.17	0.07
LG	0.64	0.49	0.06	0.04	0.32	0.11	0.07	0.04

as dramatic as the one found around the 8 Gyr peak and reveals that the environment does not lead to a thickening of the tail of the distribution corresponding to extremely quiet τ_M values. The quietness of a MW MAH defined in this way is however at odds with the observations of the LMC, whose mass is most likely above 10% of M_{MW} (Peñarrubia et al. 2016) and is at its first crossing of the viral radius (Besla et al. 2007; Kallivayalil et al. 2013). However, due to the accretion time being substantially smaller than the dynamical friction timescales, the interaction of the LMC with the Galaxy is still negligible and did not have an impact so far on its main structural properties (Mastropietro et al. 2005). In any case, our halo samples show that such a recent accretion, though being disfavoured, is also not ruled out either, and is expected to happen around 10% in constrained simulations and 15% in random ones.

4 CONCLUSIONS

In this paper the mass assembly histories of the two defining members of the Local Group (LG) – the MW and M31 – have been analyzed within the context of constrained simulations, that reproduce specific, observationally defined features of the large scale environment. Our method of constraining the initial conditions in order to produce the $z = 0$ environment is fairly accurate and is described in detail in Doumler et al. (2013a); Sorce et al. (2014); Carlesi et al. (2016a). In general, the most important cosmographic features on scales greater than ~ 5 Mpc (such as the Virgo cluster, the Local Void, etc) are reproduced with the correct density and in the correct place. Moreover, the simulated LGs lie on a filament whose properties (evaluated using the velocity shear tensor) are in good agreement with the reconstruction from the observational values of Libeskind et al. (2015b). As smaller scales remain unconstrained, LGs are not automatically reproduced. Instead random haloes form embedded within the constrained environment. The criteria to define these as so-called “LGs” are termed a “LG model”.

The first step is to introduce a LG model, namely a set of observationally motivated intervals for mass, mass ratio, isolation, relative velocity, and separation of two haloes at $z = 0$. Any pair of haloes that meet the criteria defined in the LG model are – for the purposes of this study — considered a LG. The mass assembly histories (MAH) of the LGs that form in our constrained simulations are compared with halo pairs identified in un-constrained Λ CDM simulations, run with the same Planck-I cosmological parameters, according to identical LG model. The same halo finder as well as merger tree algorithms were used on both simulations to ensure consistency between the results.

We have identified a total of 314 constrained LGs (CS sample) and 2028 LG-like pairs in the standard Λ CDM simulations

(RAN sample). We use these to characterize the MAH by computing formation times (τ_F , defined as the lookback time when the main progenitor of the halo had acquired half its $z = 0$ mass), last major merger times (τ_M , defined as the time when the halo last had a merger of at least 1 : 10) and the growth curve of the MW and M31-like haloes. This comparison can be used to isolate the effects of the environment on how LG like pairs of haloes acquire mass. Our main findings are

- The median growth of a MW or M31 halo in our constrained simulations is faster at early times compared to haloes in unconstrained LGs. The difference is statistically significant at the 1σ level. For example, MWs forming in constrained simulations acquire, in the median, 75% of their $z = 0$ mass at a lookback time of ~ 7.25 Gyr (similar values for M31). LGs identified in unconstrained simulations, acquire 75% of their mass more than a Gyr later at look back times of ~ 6 Gyr.

- As expected from above, an examination of the formation times (τ_F), reveal a similar story: their distribution for CS LGs peak at values ≈ 0.5 Gyr later than RAN ones. We examine the probability that *both* haloes have formed in the first half of the age of the Universe, which is 64% in CS compared to 49% in RAN. Formation times are only slightly affected by the environment, as the distribution functions of τ_F overlap significantly between the CS and RAN samples.

- The median last major merger times τ_M are 7.75 (MW) and 7.5 Gyr (M31), 1.5 Gyr above the CS pairs. The difference τ_M distributions obtained for CS and RAN is significant at the 99% confidence level, as given by the P-value computed with the KS-test.

The above results are in agreement with observations (e.g. Hammer et al. 2007; Ruchti et al. 2015) which place this value within the 8 – 10 Gyr interval for MW and close to the estimates of $\tau_M \approx 7 - 9$ Gyr (Hammer et al. 2010; Fouquet et al. 2012; Hammer et al. 2013) in the case of M31. Qualitatively, this tendency towards quieter merger histories associated with constrained simulations agrees with the findings of Forero-Romero et al. (2011), where a small sample of CSs was used to derive an expected $\tau_M > 10$ Gyr (lookback time) for both MW and M31. Extremely recent accretion of large satellites such as the LMC are found to take place around 10% (15%) of the times for CS (RAN) – a kind of event that would classify as a major merger according to our definition, but would nonetheless leave the properties of the Galaxy largely unaffected.

In order to examine our results in the context of empirically derived fitting formulas, we fit our MAH to Eq. (2), taken from

McBride et al. (2009). We find some differences with the best fit values of Boylan-Kolchin et al. (2010) and Forero-Romero et al. (2011), which result in a Δ_{RMS} comprised within 0.08 and 0.28 depending on the best-fit parameter set used. We believe these can be attributed to the different halo finding methods, cosmological parameters, LG models and redshift intervals used.

What we have attempted to accomplish in this work is to characterise the effect of cosmography on the history of the LG; to ask “what role does environment play on producing a merger history for a pair of LG like haloes that is consistent with observations?”. For example, if morphological characteristics (such as the existence of disks) of the MW and M31 imply that no major merger took place in *either* of the main LG galaxies during at least the last ≈ 7 Gyr, it can be said that we lived in a quiet merger history. LGs with quiet merger histories occur $\approx 27\%$ of the time in constrained environments but just 14% of the time in unconstrained environments, albeit with the exact same set of criteria applied to identify a pair of haloes as a probability twice as much larger than the naïve Λ CDM expectation, where pairs of DM haloes - defined *via* the same LG model - experience this kind of merger history at a 14% rate. We may take an even more conservative approach, and consider only those LGs without any major mergers in the last 10.5 Gyr. Roughly 6% of constrained LGs and 4% of unconstrained LGs satisfy such a criterium, a small - though not vanishing - probability and difference. To conclude, we have compared LG-like objects identified in constrained and in random simulations of the same cosmology using the same LG model, following the approach of Forero-Romero et al. (2011) but using a larger statistical sample. We have demonstrated that these samples are statistically different and therefore also the correct large scale environment as constructed in the constrained simulation plays an important role to understand the formation and evolution of our Local Group of galaxies.

ACKNOWLEDGEMENTS

EC would like to thank Giorgio Mastrota for the support and the interesting discussions. YH has been partially supported by the Israel Science Foundation (1358/18). NIL acknowledges financial support of the Project IDEXLYON at the University of Lyon under the Investments for the Future Program (ANR-16-IDEX-0005). GY and AK are supported by Ministerio de Economía y Competitividad and the Fondo Europeo de Desarrollo Regional (MINECO/FEDER, UE) in Spain through grants AYA2015-63810-P and PGC2018-094975-B-C21. AK is also supported by the Spanish Red Consolider MultiDark FPA2017-90566-REDC. He further thanks Soundgarden for badmotorfinger. SP is supported by the Russian Academy of Sciences program P-7 RAS Program of basic research 12 “Problems of Origin and Evolution of the Universe”. The standard RAN Λ CDM simulations have been performed on the local cluster of the Leibniz Institut für Astrophysik in Potsdam. We thank the Red Española de Supercomputación for granting us computing time in the Marenostrum Supercomputer at the BSC-CNS where the Local Group Factory simulations have been performed.

REFERENCES

Aragón-Calvo M. A., Neyrinck M. C., Silk J., 2016, arXiv e-

- prints, p. arXiv:1607.07881
 Aragón-Calvo M. A., Platen E., van de Weygaert R., Szalay A. S., 2010, *ApJ*, 723, 364
 Aragón-Calvo M. A., van de Weygaert R., Jones B. J. T., van der Hulst J. M., 2007, *ApJ*, 655, L5
 Avila S., Knebe A., Pearce F. R., Schneider A., Srisawat C., Thomas P. A., Behroozi P., Elahi P. J., Han J., Mao Y.-Y., Onions J., Rodriguez-Gomez V., Tweed D., 2014, *MNRAS*, 441, 3488
 Baiesi Pillastrini G. C., 2009, *MNRAS*, 397, 1990
 Benitez-Llambay A., Navarro J. F., Abadi M. G., Gottlöber S., Yepes G., Hoffman Y., Steinmetz M., 2013, *Astrophys. J.*, 763, L41
 Besla G., Kallivayalil N., Hernquist L., Robertson B., Cox T. J., van der Marel R. P., Alcock C., 2007, *ApJ*, 668, 949
 Bland-Hawthorn J., Freeman K., 2014, *The Origin of the Galaxy and Local Group*, Saas-Fee Advanced Course, Volume 37. ISBN 978-3-642-41719-1. Springer-Verlag Berlin Heidelberg, 2014, p. 1, 37, 1
 Bland-Hawthorn J., Peebles P. J. E., 2006, *Science*, 313, 311
 Boylan-Kolchin M., Bullock J. S., Kaplinghat M., 2012, *MNRAS*, 422, 1203
 Boylan-Kolchin M., Springel V., White S. D. M., Jenkins A., 2010, *MNRAS*, 406, 896
 Brook C. B., Gibson B. K., Martel H., Kawata D., 2005, *ApJ*, 630, 298
 Brook C. B., Kawata D., Gibson B. K., Freeman K. C., 2004, *ApJ*, 612, 894
 Brown T. M., et al., 2008, *ApJ*, 685, L121
 Carlesi E., Hoffman Y., Sorce J. G., Gottlöber S., 2017a, *MNRAS*, 465, 4886
 Carlesi E., Hoffman Y., Sorce J. G., Gottlöber S., Yepes G., Courtois H., Tully R. B., 2016b, *MNRAS*, 460, L5
 Carlesi E., Mota D. F., Winther H. A., 2017b, *MNRAS*, 466, 4813
 Carlesi E., Sorce J. G., Hoffman Y., Gottlöber S., Yepes G., Libeskind N. I., Pilipenko S. V., Knebe A., Courtois H., Tully R. B., Steinmetz M., 2016a, *MNRAS*, 458, 900
 Cautun M., Deason A. J., Frenk C. S., McAlpine S., 2018, *Monthly Notices of the Royal Astronomical Society*, 483, 2185
 Creasey P., Scannapieco C., Nuza S. E., Yepes G., Gottlöber S., Steinmetz M., 2015, *ApJ*, 800, L4
 Dalcanton J. J., et al., 2012, *ApJS*, 200, 18
 de Rossi M. E., Tissera P. B., De Lucia G., Kauffmann G., 2009, *MNRAS*, 395, 210
 Diaz J. D., Koposov S. E., Irwin M., Belokurov V., Evans N. W., 2014, *MNRAS*, 443, 1688
 Doumler T., Courtois H., Gottlöber S., Hoffman Y., 2013b, *MNRAS*, 430, 902
 Doumler T., Gottlöber S., Hoffman Y., Courtois H., 2013c, *MNRAS*, 430, 912
 Doumler T., Hoffman Y., Courtois H., Gottlöber S., 2013a, *MNRAS*, 430, 888
 Dressler A., 1980, *ApJ*, 236, 351
 Elahi P. J., Lewis G. F., Power C., Carlesi E., Knebe A., 2015, *MNRAS*, 452, 1341
 Fattahi A., Navarro J. F., Sawala T., Frenk C. S., Oman K. A., Crain R. A., Furlong M., Schaller M., Schaye J., Theuns T., Jenkins A., 2016, *MNRAS*, 457, 844
 Forero-Romero J. E., Hoffman Y., Bustamante S., Gottlöber S., Yepes G., 2013, *ApJ*, 767, L5
 Forero-Romero J. E., Hoffman Y., Gottlöber S., Klypin A., Yepes G., 2009, *MNRAS*, 396, 1815
 Forero-Romero J. E., Hoffman Y., Yepes G., Gottlöber S., Piontek

- R., Klypin A., Steinmetz M., 2011, MNRAS, 417, 1434
- Fouquet S., Hammer F., Yang Y., Puech M., Flores H., 2012, MNRAS, 427, 1769
- Garaldi E., Baldi M., Moscardini L., 2016, JCAP, 1, 050
- Garrison-Kimmel S., Boylan-Kolchin M., Bullock J. S., Kirby E. N., 2014, MNRAS, 444, 222
- González R. E., Kravtsov A. V., Gnedin N. Y., 2014, ApJ, 793, 91
- Gottlöber S., Hoffman Y., Yepes G., 2010, High Performance Computing in Science and Engineering. Springer Berlin Heidelberg, Berlin, Heidelberg, p. 309322
- Hahn O., Carollo C. M., Porciani C., Dekel A., 2007, MNRAS, 381, 41
- Hammer F., Puech M., Chemin L., Flores H., Lehnert M. D., 2007, ApJ, 662, 322
- Hammer F., Yang Y., Flores H., Puech M., 2012, Modern Physics Letters A, 27, 1230034
- Hammer F., Yang Y., Fouquet S., Pawlowski M. S., Kroupa P., Puech M., Flores H., Wang J., 2013, MNRAS, 431, 3543
- Hammer F., Yang Y. B., Wang J. L., Ibata R., Flores H., Puech M., 2018, MNRAS, 475, 2754
- Hammer F., Yang Y. B., Wang J. L., Puech M., Flores H., Fouquet S., 2010, ApJ, 725, 542
- Helmi A., Babusiaux C., Koppelman H. H., Massari D., Veljanoski J., Brown A. G. A., 2018, Nature, 563, 85
- Hoffman Y., Metuki O., Yepes G., Gottlöber S., Forero-Romero J. E., Libeskind N. I., Knebe A., 2012, MNRAS, 425, 2049
- Hoffman Y., Ribak E., 1991, ApJ, 380, L5
- Iorio G., Belokurov V., 2019, MNRAS, 482, 3868
- Kallivayalil N., van der Marel R. P., Besla G., Anderson J., Alcock C., 2013, ApJ, 764, 161
- Karachentsev I. D., Kashibadze O. G., Makarov D. I., Tully R. B., 2009, MNRAS, 393, 1265
- Kilic M., Munn J. A., Harris H. C., von Hippel T., Liebert J. W., Williams K. A., Jeffery E., DeGennaro S., 2017, ApJ, 837, 162
- Klypin A. A., Trujillo-Gomez S., Primack J., 2011, ApJ, 740, 102
- Knebe A., et al. 2013, MNRAS, 435, 1618
- Knollmann S. R., Knebe A., 2009, ApJS, 182, 608
- Laporte C. F. P., et al. 2018, MNRAS, 481, 286
- Leclercq F., Jasche J., Wandelt B., 2015, A&A, 576, L17
- Libeskind N. I., Hoffman Y., Tully R. B., Courtois H. M., Pomarède D., Gottlöber S., Steinmetz M., 2015a, MNRAS, 452, 1052
- Libeskind N. I., Hoffman Y., Tully R. B., Courtois H. M., Pomarède D., Gottlöber S., Steinmetz M., 2015b, MNRAS, 452, 1052
- Mastropietro C., Moore B., Mayer L., Wadsley J., Stadel J., 2005, Monthly Notices of the Royal Astronomical Society, 363, 509
- McBride J., Fakhouri O., Ma C.-P., 2009, MNRAS, 398, 1858
- Metuki O., Libeskind N. I., Hoffman Y., Crain R. A., Theuns T., 2015, MNRAS, 446, 1458
- Naab T., Ostriker J. P., 2006, MNRAS, 366, 899
- Nuza S. E., Kitaura F.-S., Heß S., Libeskind N. I., Müller V., 2014, MNRAS, 445, 988
- Parry O. H., Eke V. R., Frenk C. S., 2009, MNRAS, 396, 1972
- Peñarrubia J., Gómez F. A., Besla G., Erkal D., Ma Y.-Z., 2016, MNRAS, 456, L54
- Penzo C., Macciò A. V., Baldi M., Casarini L., Oñorbe J., Dutton A. A., 2016, MNRAS, 461, 2490
- Planck Collaboration 2014, A&A, 571, A16
- Rodríguez-Gomez V., et al., 2017, MNRAS, 467, 3083
- Ruchti G. R., et al., 2015, MNRAS, 450, 2874
- Saglia R. P., Fabricius M., Bender R., Montalto M., Lee C.-H., Riffeser A., Seitz S., Morganti L., Gerhard O., Hopp U., 2010, A&A, 509, A61
- Sales L. V., Navarro J. F., Theuns T., Schaye J., White S. D. M., Frenk C. S., Crain R. A., Dalla Vecchia C., 2012, MNRAS, 423, 1544
- Salomon J.-B., Ibata R. A., Famaey B., Martin N. F., Lewis G. F., 2016, MNRAS, 456, 4432
- Sawala T., Frenk C. S., Fattahi A., Navarro J. F., Bower R. G., Crain R. A., Dalla Vecchia C., Furlong M., Helly J. C., Jenkins A., Oman K. A., Schaller M., Schaye J., Theuns T., Trayford J., White S. D. M., 2014, ArXiv 1412.2748
- Scannapieco C., Creasey P., Nuza S. E., Yepes G., Gottlöber S., Steinmetz M., 2015, A&A, 577, A3
- Scannapieco C., White S. D. M., Springel V., Tissera P. B., 2009, MNRAS, 396, 696
- Sohn S. T., Anderson J., van der Marel R. P., 2012, ApJ, 753, 7
- Sorce J. G., 2015, MNRAS, 450, 2644
- Sorce J. G., Courtois H. M., Gottlöber S., Hoffman Y., Tully R. B., 2014, MNRAS, 437, 3586
- Sorce J. G., Gottlöber S., Yepes G., Hoffman Y., Courtois H. M., Steinmetz M., Tully R. B., Pomarède D., Carlesi E., 2016, MNRAS, 455, 2078
- Srisawat C., et al. 2013, MNRAS, 436, 150
- Stewart K. R., Bullock J. S., Wechsler R. H., Maller A. H., Zentner A. R., 2008, ApJ, 683, 597
- Stinson G. S., Bailin J., Couchman H., Wadsley J., Shen S., Nickerson S., Brook C., Quinn T., 2010, MNRAS, 408, 812
- Tasitsiomi A., Kravtsov A. V., Gottlöber S., Klypin A. A., 2004, ApJ, 607, 125
- Tollerud E. J., Boylan-Kolchin M., Bullock J. S., 2014, MNRAS, 440, 3511
- Toth G., Ostriker J. P., 1992, ApJ, 389, 5
- Tully R. B., Courtois H., Hoffman Y., Pomarède D., 2014, Nature, 513, 71
- van der Marel R. P., Fardal M. A., Sohn S. T., Patel E., Besla G., del Pino A., Sahlmann J., Watkins L. L., 2019, ApJ, 872, 24
- van Dokkum P. G., et al., 2013, ApJ, 771, L35
- Wang H., Mo H. J., Yang X., Zhang Y., Shi J., Jing Y. P., Liu C., Li S., Kang X., Gao Y., 2016, ApJ, 831, 164
- Wang Y., Pearce F. R., Knebe A., Schneider A., Srisawat C., Tweed D., Jung I., Han J., Helly J., Onions J., Elahi P. J., Thomas P. A., Behroozi P., Yi S. K., Rodríguez-Gomez V., Mao Y.-Y., Jing Y., Lin W., 2016, MNRAS, 459, 1554
- White S. D. M., Rees M. J., 1978, MNRAS, 183, 341
- Zavala J., Avila-Reese V., Firmani C., Boylan-Kolchin M., 2012, MNRAS, 427, 1503

This paper has been typeset from a $\text{\TeX}/\text{\LaTeX}$ file prepared by the author.

APPENDIX A: METROC++ – A PARALLEL CODE FOR THE COMPUTATION OF MERGER TREES IN COSMOLOGICAL SIMULATIONS

METROC++ is an acronym that stands for *M*Erger *T*rees *O*n *C*++. The name is reference to the infamous third subway line (Metro C) in Rome (where EC grew up) and whose assembly (still undergoing, by the time this paper is being submitted) is taking an amount of time comparable to the formation of a dark matter halo. It is a C++11 code designed to compute merger trees in cosmological simulations, that uses MPI-2.0 C bindings for

the implementation of distributed-memory parallelism. The code uses particle IDs to match haloes and is able to track them among non-consecutive snapshots in order to cope with the shortcomings of the halo finders when dealing with subhaloes. These are two of the three properties suggested by Srisawat & et al. (2013), the third one, namely the ability of smoothing over large fluctuations in halo mass, has not been implemented in the code and has been done in the post-processing stage. A practical description of the usage of the code can be found in the user's guide ⁴ that is provided with it. Here we will only deal with the main features of the algorithms and the physical assumptions of the code.

A1 Parallelization strategy

The simulation volume is split into N^3 sub-cubes, where N is a user-defined number that should be chosen ensuring that $L/N > 2.0h^{-1}\text{Mpc}$ (L is the box size). This volume splitting is performed only in the case of full box cosmological simulations, as the *zoom-in* optimization of the code relies on a purely *serial* version of the algorithm. Each task is assigned a (comoving) sub-volume of the simulation box comprised of $\approx N/N_{task}$ cells. Halo properties with their particle ID content are then retrieved from two catalogs at the time (corresponding to two redshifts z_i and z_{i+1} , with $z_{i+1} > z_i$) and assigned to each task according to their position in space. The cells at the edge of every sub-volume constitute a buffer zone that tasks communicate to their neighbours to ensure that the haloes will be then consistently compared to *all* of their potential progenitors. While a larger grid cell (smaller N) might result in a better reconstruction of the trees, enlarging the list of potential progenitors, it also means that the buffers to be communicated among the tasks are larger, slowing down the execution of the program and increasing the memory request. On the other hand, smaller grid cells (larger N) lead to a speed-up of the code execution and reduce memory consumption at the expense of accuracy. It is up to the user to decide how to balance this trade-off. In the present paper, we selected $N = 48$ for the computation of the RAN merger trees after checking for convergence, that is, ensuring that the results produced would not change for $N < 48$.

A2 Tree building and halo tracking

After all haloes with their particle ID content have been correctly read and distributed, each task produces a `map` ⁵ linking the particle ID to the `vector` of halo IDs to which it belongs to. In this way, a single particle might be assigned to more haloes at the same time - e.g. a sub-halo and its host. The maps are produced for both the i -th and $i + 1$ -th catalogs on each task and their particle ID content

is compared to identify the halo connections, which are established only among objects sharing at least N_{min} (user defined) particles. For each halo A at z_i with N_A particles, sharing at least N_{min} particles with N' haloes at z_{i+1} , we compute the merit function (see Knebe & et al. 2013):

$$\sum_{j=0}^{N'} M(N_A, N_j) = \frac{N_{A,j}}{N_A, N_j} \quad (\text{A1})$$

where N_j is the number of particles of the j -th possible progenitor. The comparisons are carried for $z_i \rightarrow z_{i+1}$ (forwards) and $z_{i+1} \rightarrow z_i$ (backwards), and all the connections above N_{min} are ranked using Eq. (A1) and sorted in descending order. A halo h_j is labeled as progenitor of h_A if the latter maximizes the former's merit function, ensuring that haloes have a *unique* descendant and they do not split. If a halo is left with no likely progenitor, and provided it is composed by a number of particles above a user-specified threshold, it is labeled as *orphan* and the code still keeps track of its particle ID content for comparison during the following snapshots. This enables to reconnect subhaloes with their progenitor at a non-subsequent snapshot if the halo finder fails to identify it at any step, which typically happens when a subhalo is orbiting close to the center of mass of its host (Avila et al. 2014; Wang et al. 2016). During the time steps in which the halo has been missing, the code replaces it with a token halo with exactly the same properties of the last valid descendant, until a proper descendant is can be identify. After a (user specified) maximum number of steps, if no progenitor can be found for an orphan halo, the particle content is dropped and the merger tree is truncated.

At each step, once the pairwise catalog comparison has finished, the code runs a check on the halos in the buffer zone (which might have been assigned to a different descendant on each task) to ensure that they are correctly assigned to their a unique descendant. Then, the list of halos at z_i are printed to a single output file together with their rank-ordered (by the merit function) descendants at z_{i+1} .

With the code it is also provided a series of scripts that allow to reconstruct the merging histories reading from the ASCII output files and store them into a SQL database that can be queried using the $z = 0$ ID of the halos.

⁴ <https://github.com/EdoardoCarlesi/MetroCPP/blob/master/doc/UG.pdf>

⁵ According to <http://www.cplusplus.com/> a `map` is an *associative container that stores elements formed by a combination of a key value and a mapped value, following a specific order*. In practice, we can use a `map` as an array whose element are not to be called by integer values but rather by *keys* of arbitrary type. Defining a `particleHaloMap` linking `particleID` to `haloID` we can quickly retrieve the ; e.g. if `particleID= 12345` and `haloID= 6789` then `particleHaloMap[12345]` will return 6789. This property makes the process of comparing very large arrays of particle IDs extremely quick, at the price of a larger memory requirements.